Dynamic Nature of High-Pressure Ice VII

Qi-Jun Ye,[1] Lin Zhuang,[1] and Xin-Zheng Li[1,2,3,*]

[1]State Key Laboratory for Artificial Microstructure and Mesoscopic Physics, Frontier Science Center for Nano-optoelectronics and School of Physics, Peking University, Beijing 100871, People's Republic of China
[2]Interdisciplinary Institute of Light-Element Quantum Materials, Research Center for Light-Element Advanced Materials, and Collaborative Innovation Center of Quantum Matter, Peking University, Beijing 100871, People's Republic of China
[3]Peking University Yangtze Delta Institute of Optoelectronics, Nantong, Jiangsu 226010, People's Republic of China

(Received 26 November 2020; revised 10 February 2021; accepted 31 March 2021; published 3 May 2021)

Starting from Shannon's definition of dynamic entropy, we propose a theory to describe the rare-event-determined dynamic states in condensed matter and their transitions and apply it to high-pressure ice VII. A dynamic intensive quantity named dynamic field, rather than the conventional thermodynamic intensive quantities such as temperature and pressure, is taken as the controlling variable. The dynamic entropy versus dynamic field curve demonstrates two dynamic states in the stability region of ice VII and dynamic ice VII. Their microscopic differences were assigned to the dynamic patterns of proton transfer. This study puts a similar dynamical theory used in earlier studies of glass models on a simpler and more fundamental basis, which could be applied to describe the dynamic states of more realistic condensed matter systems.

DOI: 10.1103/PhysRevLett.126.185501

Matter exists in the form of states, wherein the physical properties vary continuously before abrupt changes happen upon transitions [1]. Abundant states have constituted our understanding of matter from different aspects, such as crystal states characterized by atomic structures [2,3] and superconductors and charge density waves characterized by electronic structures [4–7]. Recent years have witnessed considerable progress on simulating these states, especially the ones characterized by atomic structures, along with thorough exploration of rare events and their dynamics [8,9]. Here, rare events mean dynamic activities occurring out of equilibrium and with constraints; e.g., atom A cannot move until atom B moves out of the way [10] and the ice rule [11]. Description of these dynamic states and their transitions using conventional thermodynamics, however, is difficult.

One prominent example exists in high-pressure (P) ice. At P's of 2–80 GPa and ~500 K, its states of matter are dominated by akin body-centered-cubic (bcc) structures, e.g., ice VII, dynamic ice VII, and superionic (SI) ice [12–20]. Conventionally, these states can be attributed to solid with atoms localized in the crystalline sites [Fig. 1(a)] or liquid with atoms traveling ergodically over the whole configurational space [Fig. 1(b)]. The so-called dynamic ice VII, however, presents an in-between feature; i.e., protons are localized on their sites but can occasionally hop to others in a timescale of picoseconds and longer [Fig. 1(c)]. It was considered as a distinct state from ice VII in earlier studies [Fig. 1(d)], due to the occurrence of dynamical translational disorder (proton hopping along hydrogen bonds) [13,15]. One may intuitively interpret this as the protons cannot be transferred in ice VII and can in dynamic ice VII. However, this criterion is questionable, as the structures of the bcc skeleton of oxygens remain the same and there is no transient change in the structural order or thermodynamic properties [Fig. 1(e) and Refs. [21–23]]. A paradox arises: If the timescale is long enough, proton

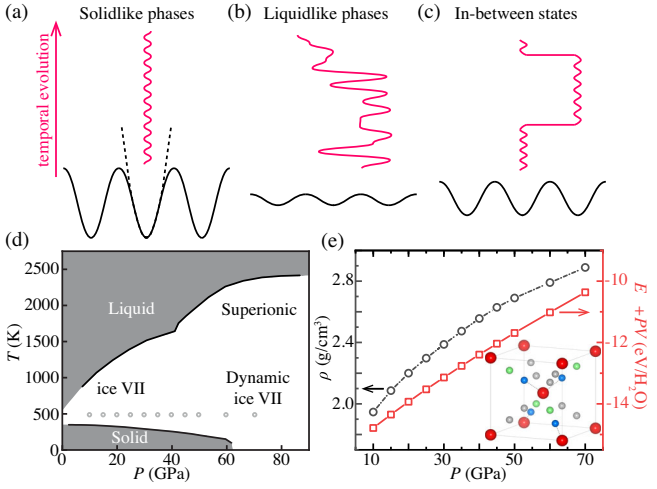

FIG. 1. (a) Solid, (b) liquid, and (c) the in-between state. (d) The phase diagram of bcc ice. There are well-defined solid and liquid states in the shadowed region, while in the white region the boundaries between ice VII, dynamic ice VII, and SI remain controversial. (e) Density and thermodynamic state function at 500 K. Inset: bcc ice structure. In the bcc skeleton formed by oxygen (red), protons intersperse in the covalent sites (blue) of neighboring oxygen pairs. The equivalent sites (green) can be occupied through transfer motions. The other sites (gray) consist in another hydrogen bonding network.

transfer can also occur in ice VII. Consequently, ice VII and dynamic ice VII should be considered as a single state where proton transfer can occur in the long time limit, though with large numerical variances in the transfer rates.

In this Letter, we present a theory to describe the dynamic states determined by rare events and their transitions, starting merely from Shannon's definition of the dynamic entropy, and apply it to high-P ice VII. By dividing the space into pieces of components, we decompose the atomic trajectories of protons into intracomponent localized motions and intercomponent diffusive motions. The dynamic field, a central quantity in the dynamic partition function, is taken as the controlling variable for the intercomponent motions. This field can reveal the different patterns of dynamic motions related to dynamic constraint and, hence, the transitions between dynamic states. In the simulations, we derived its values for each P by mapping to a constructed ensemble, nominated as an isostructural isodynamic ensemble. Two states were discriminated using the dynamic entropy versus dynamic field curve in the stability region of high-P ice VII, and a turning P is obtained by approaching the simulation results to the long time limit. By resorting to the potential energy surface (PES), the mechanism underlying this transition is detailed.

We start with descriptions of the dynamic properties. In previous studies, the diffusion coefficient was taken as the order parameter in discriminating static and dynamic ice VII [9,24–26]. Considering the rare-event nature of proton transfer at low temperatures (T), we resort to a fundamental property, the proton motions. There are two types: (i) liquidlike diffusive motion as a proton transfers to another equivalent site; (ii) solidlike localized motion as a proton oscillates around its own equilibrium site. The essential dynamical information is muffled by thermal noises, since the diffusive motions are rare compared to the localized motions. In order to highlight the diffusive motions, the concept of "components" is introduced [27]. One component is a close set of neighboring phase points containing a local minimum of the PES:

$$\Omega = \cup_\alpha \Omega_\alpha, \quad \text{with} \quad \Omega_\alpha = \{(\boldsymbol{x}, \boldsymbol{p}) \in \Omega_\alpha\}. \tag{1}$$

Ω represents the whole phase space, and Ω_α is the component. The components are assumed to have a confinement condition (atoms stay in one component for a long time) and internal ergodicity [27]. We define them using Voronoi decomposition, by constructing the Wigner-Seitz cell of the equivalent sites [28]. Upon this, we can describe the diffusive motions by intercomponent hoppings, with each being called an activity. The activity rate k is defined by the number of activities K occurring in a single component and a certain observation time t_{obs}, with $k = K/t_{\text{obs}}$. Extensive dynamic quantities scale with t_{obs}, but, when no ambiguity exists, we omit t_{obs} in the equations.

The core quantity to describe a system is its partition function and the relevant degrees of freedom (d.o.f.). Thermodynamic-intensive quantities, e.g., T and P, are the conventional choice to identify the equilibrium states. In bcc ice, however, the diffusion coefficient presents gradual changes in a wide range of T's and P's, while discontinuous change in structural order and state function cannot be observed. This implies that an extra d.o.f. other than T and P should be resorted to. Here, we employ a dynamic form of the partition function and use an extra d.o.f. named "dynamic field(s)". It was introduced first in studies of glass transition as an auxiliary field for enhanced and reduced sampling [29–35]. By interpreting glass transition as a space-time phase transition, Hedges *et al.* proposed that s is its controlling variable [33]. This s, however, was a pure predefined mathematical tool, and this scheme is limited to glass models. We derive the value of s for each (T, P) by mapping to a constructed ensemble and, hence, extend this dynamical theory to realistic bcc ice, as detailed later.

Following the thermodynamic convention, we write the partition function of the isodynamic ensemble (with the same s, named analogously from isothermal ensemble) in the form of the sum of probabilities

$$Z_D(s) = \sum_K p(s, K) \tag{2}$$

to find the system in particular dynamic states. The partition according to K is applied [36]. The subscript D denotes dynamics. Equation (2) becomes $Z_0 = \sum_K p_0(K)$ when $s = 0$, where $p_0(K)$ is the unbiased distribution. When one applies a finite s, $p(s, K)$ takes the form of $p_0(K)e^{-s\cdot K}$ by making analogy to the thermodynamic formula in earlier studies [33,38,39]. Here, we note that an elegant mathematical form of the dynamic partition function can be derived by using merely the information theory [40]. According to Shannon [41], the dynamic entropy within t_{obs} is

$$S_D(s) = -\sum_K p(s, K) \ln p(s, K). \tag{3}$$

A reasonable $p(s, K)$ should give statistical results consistent with the observed ones; i.e., $p(s, K)$ and $\langle K \rangle_s = \sum_K p(s, K) \cdot K$ must conform to $p_0(K)$ and K_0 when $s = 0$. The variation of $p(s, K)$ subjected to the least bias estimation from known results and the maximum of entropy S_D [40] is

$$\delta\left\{ S_D(s) + \sum_K \lambda_{1,K}[p(s, K) - p_0(K)] + \lambda_2[\langle K \rangle_s - K_0] \right\} = \sum_K \delta p(s, K)\{-[\ln p(s, K) + 1] + \lambda_{1,K} + \lambda_2 K\} = 0, \tag{4}$$

which leads to

$$p(s,K) \sim e^{-(\lambda_{1,K}-1)-\lambda_2 K}. \tag{5}$$

Here, $\lambda_{1,K}$ and λ_2 are the Lagrange multipliers of constraint. If we define $s = \lambda_2$ and the implicit-K part as $p_0(k)$, we have

$$p(s,K) \equiv p_0(K)e^{-s\cdot K}. \tag{6}$$

The dynamic partition function

$$Z_D(s) = \sum_K e^{-s\cdot K} p_0(K) \tag{7}$$

is then obtained.

The dynamic field can reveal the intrinsic correspondence among different thermodynamic configurations. Dynamic properties are fundamentally controlled by s, through $\langle K\rangle_s = \partial Z_D(s)/\partial s$. Therefore, upon artificially changing s, Hedges *et al.* claimed that for each (T,P) the system would experience a transition between the active and inactive states [33]. In our cases, the principal common ground between ice VII and dynamic ice VII is their bcc structure. Correspondingly, we found that similar s dependencies of $Z_D(s)$ among different (T,P)'s exist, which can reveal their internal connection on dynamics. To quantify this, we resort to an isostructural isodynamic ensemble. In front of the aforementioned isodynamic, we put a word "isostructural" to emphasize the geometric requirement, i.e., the states within the region of ice VII and dynamic ice VII. This ensemble contains all the information of thermodynamic and dynamic states of interest. Therefore, it can describe the transition between states within this bcc region. It consists of multiple subensembles, and its partition function can be derived accordingly, as

$$\begin{aligned} Z_{\mathrm{bcc}}(s) &= \sum_{(T,P),\mathrm{bcc}} Z_{D,(T,P)}(s)\cdot e^{-\beta G(T,P)} \\ &= \sum_K e^{-s\cdot K} \sum_{(T,P),\mathrm{bcc}} p_{0,(T,P)}(K) e^{-\beta G(T,P)} \\ &\sim \sum_K p_{\mathrm{bcc}}(s,K). \end{aligned} \tag{8}$$

$Z_{D,(T,P)}$ represents the subsequent isodynamic ensemble for one (T,P), and $e^{-\beta G(T,P)}$ is its thermodynamic weight. $G(T,P)$ is the Gibbs free energy per component. From Eq. (8),

$$p_{\mathrm{bcc}}(s,K) = \frac{1}{Z_{\mathrm{bcc}}(s)} e^{-s\cdot K} \sum_{(T,P),\mathrm{bcc}} p_{0,(T,P)}(K) e^{-\beta G(T,P)} \tag{9}$$

can be derived and then $S_{D,\mathrm{bcc}}(s)$ can be calculated. A detailed derivation of Eq. (8) is shown in Ref. [42]. Using a mapping from the unbiased $Z_{D,(T,P)}(s=0)$ to $Z_{\mathrm{bcc}}(s)$, a referenced dynamic field s_{ref} is determined for each (T,P). The rule is to ensure that the expectation value of the isostructural isodynamic ensemble at $s = s_{\mathrm{ref}}(T,P)$ equals its unbiased correspondence, i.e.,

$$\langle k\rangle_{Z_{D,(T,P)}(s=0)} = \langle k\rangle_{Z_{\mathrm{bcc}}[s=s_{\mathrm{ref}}(T,P)]}. \tag{10}$$

k is taken here to determine s_{ref}, while choices of other dynamic quantities are also allowed. This scheme enables learning the transition between different dynamic states solely from s_{ref}.

In order to sample the trajectory space, we performed extensive molecular dynamic (MD) simulations. This is doable only recently with machine learning potentials [26,48]. The simulation of each (T,P) contains samplings up to 1×10^7 time steps and a timescale of a few nanoseconds. For simulation details, please see Ref. [42]. The protons are assigned to their components at each time step [Figs. 2(a)–2(c)]. The trajectories are decomposed into intracomponent localized motions [Fig. 2(c), horizontal solid lines] and intercomponent diffusive motions [Fig. 2(c), dashed lines]. We count the number of activities at each component and present the total distribution $p_0(K)$ in Fig. 2(d). At 10–30 GPa, $p_0(K)$ concentrates at $K=0$ and falls sharply at nonzero values, since few proton transfers happen. Above 40 GPa, there are rate peaks at finite K, which extend to higher values of K with increasing P, due to easier proton transfers. Consistent with this, the inactive sites dominate at low P, whose ratio gradually drops to zero at high P [the inset in Fig. 2(d)]. S_D shows two distinct parts [Fig. 2(e)]. However, the gradual transition

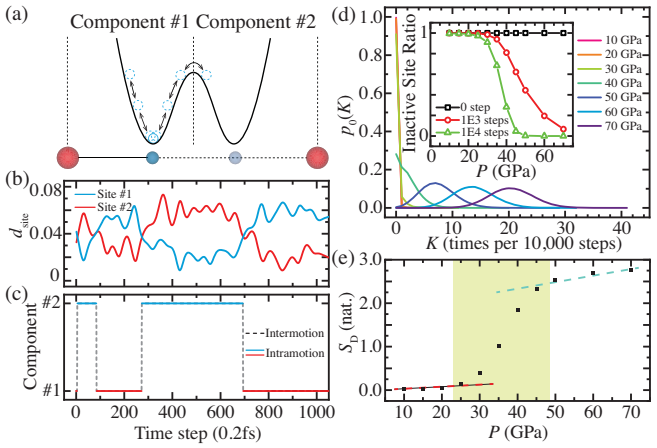

FIG. 2. (a) Schematic of the PES of proton transfer, (b) the realistic trajectory in coordinate space, and (c) the trajectory in component space. d_{site} is the distance of the proton to its equilibrium position inside each component, in the unit of fractional coordinate of the simulation cell. (d) $p_0(K)$ at different Ps with $t_{\mathrm{obs}} = 2$ ps (10 000 steps). The inset in (d) shows the t_{obs} dependence of the percentage of inactive sites for $K(t)=0$. (e) S_D computed from $p_0(K)$. The dashed lines and shadowed region are guides for the eye.

with wide P range [Fig. 2(e), shadowed region], which does not disappear with increasing the simulation scale, is beyond the scope of P-controlled phase transition (where the transition should be abrupt in P). In other words, P can reveal the dynamic difference of these states, but a native dynamic perspective is more requisite.

One unique perspective in describing such a transition is offered by s. When s is increased (decreased), the activities are suppressed (enhanced) [Eq. (7)]. This trend applies to all P's. However, there are two different s dependencies. $Z_{D,(T,P)}(s)$ and $\langle k\rangle$ are insensitive to s at low P, while they can be motivated by lowering s at high P, as shown by the almost horizontal lines at low P and the finite slopes at high P in Figs. 3(a) and 3(b). This qualitative difference can be visualized better via the S_D versus s_{ref} curve in Fig. 3(c). There are two distinct regions: a large-s_{ref} region with nearly zero S_D, mapping to low P, and a small-s_{ref} region with rapidly increased S_D, mapping to high P. The change in slope becomes sharper with increasing t_{obs}. Because of the limited sampling scale, the transition point is practically determined by the intersection of extrapolated lines of two ends at a finite t_{obs} (Fig. S7 [42]). Its dependencies on t_{obs} can be well fitted by an exponential form [inset in Fig. 3(c)]. The converged value for $t_{\mathrm{obs}} \to \infty$ is $s_{\mathrm{tran}} = -0.37$, mapping to $P \approx 32$ GPa. This is consistent with the one predicted by $p_{\mathrm{bcc}}(s, K)$ and $p_{\mathrm{bcc}}(s, T, P)$; see details in Ref. [42]. The P is also consistent with Ref. [24]. As the proton transfer might be induced by quantum tunneling, there should be a correction on s_{tran} by considering quantum nuclear effects (QNEs). Recently, tremendous progress was made in simulations of short time dynamics with QNEs included, using methods like centroid MD and ring polymer MD [49–53]. Long time simulations, however, are still challenging. Here, we use a moderate T (500 K), focus on presenting a theory to describe dynamic states, and leave QNEs for future studies. We also note that s_{tran} may not mean a phase transition point. It is more like a weaker singularity as the crossover of different dynamic states [54,55]. Clarification of its nature is also required in future studies.

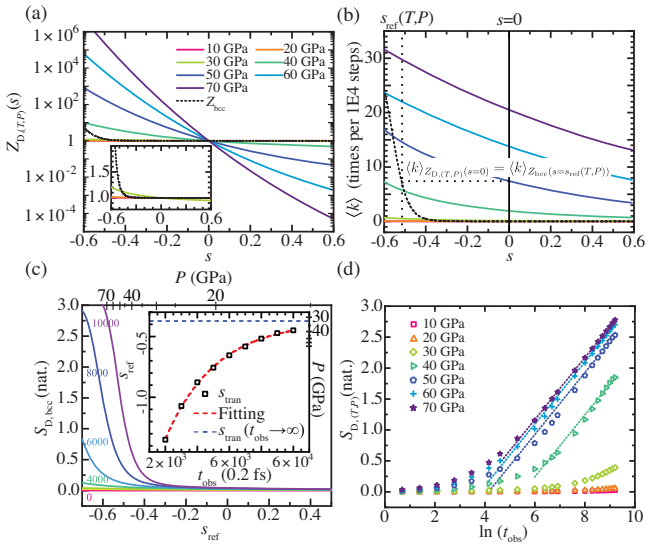

FIG. 3. (a) The partition function of the isodynamic ensembles and (b) $\langle k\rangle$ as their ensemble averages at different P's and 500 K. (a) and (b) share the legend. All the data are presented with $t_{\mathrm{obs}} =$ 2 ps (10 000 steps). (c) The $S_{D,\mathrm{bcc}}$ with different t_{obs} (in the unit of steps). Inset in (c): the tendency of transition point s_{tran} toward the long time limit. (d) The tendency of $S_{D,(T,P)}$ on t_{obs}. The dashed lines show theoretical results of Eq. (11).

The behavior of $S_D(t_{\mathrm{obs}})$ toward the long time limit roots in homogeneity. When the system is dynamically homogeneous, the activities are uniformed, wherein $S_D(t_{\mathrm{obs}})$ can be derived (pp. 15–17 in Ref. [42]), as

$$S_D(t_{\mathrm{obs}}) = \frac{1}{2}\ln\, t_{\mathrm{obs}} + \mathrm{const.} \tag{11}$$

Otherwise, $S_D(t_{\mathrm{obs}})$ is in between the static limit as $\mathcal{O}(0)$ and the homogeneous limit in Eq. (11). At high P, $S_D(t_{\mathrm{obs}})$'s converge to Eq. (11) [Fig. 3(d)]. The required t_{obs} to demonstrate this is reduced for higher P, consistent with lower s_{ref}. At low P, $S_D(t_{\mathrm{obs}})$'s are greatly off the ln t_{obs} trend, and the system is dynamically inhomogeneous. When $t_{\mathrm{obs}} \to \infty$, the high-$P$ end retains the shape, as their $S_D(t_{\mathrm{obs}})$'s differ by only a time-independent constant and are uniformly lifted by $\frac{1}{2}\ln\, t_{\mathrm{obs}}$. The low-$P$ end, however, remains flat. The crossing region witnesses a gradual change, indicating its high-order nature.

Now we detail the proton transfer mechanisms by analyzing the PES. Dynamic constraint is of central importance. The realistic barrier does not produce absolute confinement; thus, the proton is accessible to another component at $t_{\mathrm{obs}} \to \infty$. When this happens, the system is driven to an energetically uncomfortable state with the ice rule temporarily broken [Fig. 4(a), solid line]. Two routes exist to restore the ice rule, via a retrieving motion of the same proton [Fig. 4(a), dashed line] or via collective motions of more protons [Fig. 4(b), solid line]. When s_{ref} is large (the dynamic constraint is strong), the system prefers the former. This can be visualized by the PES [Fig. 4(c)], as the neighboring protons are unwilling to join the transfer. A contrast case exists when s_{ref} is small (the dynamic constraint is loosened), and the system prefers the latter. As shown by the flat bottom in Fig. 4(d), the neighboring protons are allowed to join a collective transfer [56,57]. These can also be seen via the coordination number of oxygens [42], as oxygens with 4- and 0-bonded protons appear only at high P.

Structure almost determines dynamics, establishing a convention that thermodynamic quantities native for equilibrium phase transitions are used to describe transition between different dynamic states. However, this fails when rare events are important. Our scheme demonstrates the power of the dynamic field in describing the nature of

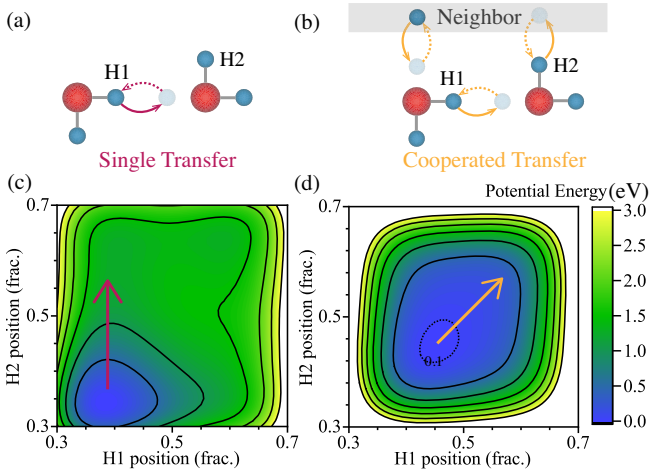

FIG. 4. Schematic of the dynamic constraint. When a single transfer occurs [solid line in (a)], there can be two paths to restore the ice rule: (a) the retrieving motion (dashed line) upon strong constraint and (b) the collective motion upon loosened constraint. (c) and (d) show the PES upon the transfer of H1 and H2 at 10 and 70 GPa, respectively.

dynamic states when they are determined by rare events and their transitions. Beyond this, the dynamic field also offers a numerical approach to access the dynamic constraint, by providing guidance on where different dynamic mechanisms exist. Despite the dynamic field being derived here numerically, it is of profound theoretical significance in future studies to specify its microscopic interpretation (analogous to those of T and P), based on which one can define the dynamic states rigorously as dynamic phases. It should also be noted that such analysis can apply to more realistic systems other than bcc ice, e.g., the hexagonal close-packed Fe system with a strong premelting effect [58] and the cubic Ca system with 1D cooperative diffusion [59]. Considering the ubiquity of dynamic constraint, we believe that this theory will bring new understanding to the fundamental question of the dynamic nature of condensed matter.

The authors are supported by the National Science Foundation of China under Grants No. 11934003, No. 11774003, and No. 11634001, the National Basic Research Programs of China under Grant No. 2016YFA0300900, Beijing Natural Science Foundation under Grant No. Z200004, and the Strategic Priority Research Program of the Chinese Academy of Sciences Grant No. XDB33010400. X.-Z. L. thanks Haitao Quan and Xinguo Ren for helpful discussions. Computational resources were provided by the High-Performance Computing Platform of Peking University, China.

*xzli@pku.edu.cn

[1] L. D. Landau, Phys. Z. Sowjetunion **11**, 26 (1937).
[2] J. F. Scott, Rev. Mod. Phys. **46**, 83 (1974).
[3] R. A. Cowley, Phys. Rev. B **13**, 4877 (1976).
[4] W. L. McMillan, Phys. Rev. B **14**, 1496 (1976).
[5] J. Bardeen, L. N. Cooper, and J. R. Schrieffer, Phys. Rev. **108**, 1175 (1957).
[6] G. Grüner, Rev. Mod. Phys. **60**, 1129 (1988).
[7] D. S. Fisher, M. P. A. Fisher, and D. A. Huse, Phys. Rev. B **43**, 130 (1991).
[8] B. Peters, in *Reaction Rate Theory and Rare Events* (Elsevier, Amsterdam, 2017), pp. 1–619.
[9] J.-A. Hernandez and R. Caracas, Phys. Rev. Lett. **117**, 135503 (2016).
[10] R. G. Palmer, D. L. Stein, E. Abrahams, and P. W. Anderson, Phys. Rev. Lett. **53**, 958 (1984).
[11] J. D. Bernal and R. H. Fowler, J. Chem. Phys. **1**, 515 (1933).
[12] M. Benoit, D. Marx, and M. Parrinello, Nature (London) **392**, 258 (1998).
[13] M. Benoit, A. H. Romero, and D. Marx, Phys. Rev. Lett. **89**, 145501 (2002).
[14] A. F. Goncharov, V. V. Struzhkin, H.-k. Mao, and R. J. Hemley, Phys. Rev. Lett. **83**, 1998 (1999).
[15] A. F. Goncharov, N. Goldman, L. E. Fried, J. C. Crowhurst, I. Feng W. Kuo, C. J. Mundy, and J. M. Zaug, Phys. Rev. Lett. **94**, 125508 (2005).
[16] E. Schwegler, M. Sharma, F. Gygi, and G. Galli, Proc. Natl. Acad. Sci. U.S.A. **105**, 14779 (2008).
[17] L. E. Bove, S. Klotz, T. Strässle, M. Koza, J. Teixeira, and A. M. Saitta, Phys. Rev. Lett. **111**, 185901 (2013).
[18] M. Guthrie, R. Boehler, C. A. Tulk, J. J. Molaison, A. M. dos Santos, K. Li, and R. J. Hemley, Proc. Natl. Acad. Sci. U.S.A. **110**, 10552 (2013).
[19] M. Millot, F. Coppari, J. R. Rygg, A. Correa Barrios, S. Hamel, D. C. Swift, and J. H. Eggert, Nature (London) **569**, 251 (2019).
[20] J.-A. Queyroux, J.-A. Hernandez, G. Weck, S. Ninet, T. Plisson, S. Klotz, G. Garbarino, N. Guignot, M. Mezouar, M. Hanfland, J.-P. Itié, and F. Datchi, Phys. Rev. Lett. **125**, 195501 (2020).
[21] R. J. Hemley, A. P. Jephcoat, H. K. Mao, C. S. Zha, L. W. Finger, and D. E. Cox, Nature (London) **330**, 737 (1987).
[22] E. Wolanin, P. Pruzan, J. C. Chervin, B. Canny, M. Gauthier, D. Häusermann, and M. Hanfland, Phys. Rev. B **56**, 5781 (1997).
[23] P. Loubeyre, R. LeToullec, E. Wolanin, M. Hanfland, and D. Hausermann, Nature (London) **397**, 503 (1999).
[24] J.-A. Hernandez and R. Caracas, J. Chem. Phys. **148**, 214501 (2018).
[25] K. Komatsu, S. Klotz, S. Machida, A. Sano-Furukawa, T. Hattori, and H. Kagi, Proc. Natl. Acad. Sci. U.S.A. **117**, 6356 (2020).
[26] L. Zhuang, Q.-J. Ye, D. Pan, and X.-Z. Li, Chin. Phys. Lett. **37**, 043101 (2020).
[27] R. Palmer, Adv. Phys. **31**, 669 (1982).
[28] E. Wigner and F. Seitz, Phys. Rev. **43**, 804 (1933).
[29] P. G. Debenedetti and F. H. Stillinger, Nature (London) **410**, 259 (2001).
[30] M. Merolle, J. P. Garrahan, and D. Chandler, Proc. Natl. Acad. Sci. U.S.A. **102**, 10837 (2005).
[31] R. L. Jack, J. P. Garrahan, and D. Chandler, J. Chem. Phys. **125**, 184509 (2006).

[32] J. P. Garrahan, R. L. Jack, V. Lecomte, E. Pitard, K. van Duijvendijk, and F. van Wijland, Phys. Rev. Lett. **98**, 195702 (2007).
[33] L. O. Hedges, R. L. Jack, J. P. Garrahan, and D. Chandler, Science **323**, 1309 (2009).
[34] D. Chandler and J. P. Garrahan, Annu. Rev. Phys. Chem. **61**, 191 (2010).
[35] J. P. Garrahan and I. Lesanovsky, Phys. Rev. Lett. **104**, 160601 (2010).
[36] Here, we distinguish the trajectories by the number of activities, not by their specific processes. For example, trajectories LTL and LLT (where L and T represent the local and transfer motion, respectively) belong to the same partition with activity $K = 1$. There can be finer partitions for the trajectory space and corresponding partition function and entropy such as the well-known Kolmogorov-Sinai entropy [37].
[37] A. N. Kolmogorov, C. R. (Doklady) Acad. Sci. URSS (N.S.) **124**, 754 (1959).
[38] J. P. Eckmann and D. Ruelle, Rev. Mod. Phys. **57**, 617 (1985).
[39] V. Lecomte, C. Appert-Rolland, and F. van Wijland, J. Stat. Phys. **127**, 51 (2007).
[40] E. T. Jaynes, Phys. Rev. **106**, 620 (1957).
[41] C. E. Shannon, Bell Syst. Tech. J. **27**, 379 (1948).
[42] See Supplemental Material at http://link.aps.org/supplemental/10.1103/PhysRevLett.126.185501 for details of the method and computational setups, as well as additional discussions, which includes Refs. [43–47].
[43] G. Kresse and J. Furthmüller, Phys. Rev. B **54**, 11169 (1996).
[44] G. Kresse and D. Joubert, Phys. Rev. B **59**, 1758 (1999).
[45] J. Sun, R. C. Remsing, Y. Zhang, Z. Sun, A. Ruzsinszky, H. Peng, Z. Yang, A. Paul, U. Waghmare, X. Wu, M. L. Klein, and J. P. Perdew, Nat. Chem. **8**, 831 (2016).
[46] D. P. Kingma and J. Ba, arXiv:1412.6980.
[47] S. Plimpton, J. Comput. Phys. **117**, 1 (1995).
[48] H. Wang, L. Zhang, J. Han, and W. E, Comput. Phys. Commun. **228**, 178 (2018).
[49] A. Witt, S. D. Ivanov, M. Shiga, H. Forbert, and D. Marx, J. Chem. Phys. **130**, 194510 (2009).
[50] S. Habershon, D. E. Manolopoulos, T. E. Markland, and T. F. Miller, Annu. Rev. Phys. Chem. **64**, 387 (2013).
[51] J. S. Cao and G. A. Voth, J. Chem. Phys. **100**, 5093 (1994).
[52] A. Pérez, M. E. Tuckerman, and M. H. Müser, J. Chem. Phys. **130**, 184105 (2009).
[53] M. Rossi, M. Ceriotti, and D. E. Manolopoulos, J. Chem. Phys. **140**, 234116 (2014).
[54] L. Xu, P. Kumar, S. V. Buldyrev, S.-H. Chen, P. H. Poole, F. Sciortino, and H. E. Stanley, Proc. Natl. Acad. Sci. U.S.A. **102**, 16558 (2005).
[55] G. G. Simeoni, T. Bryk, F. A. Gorelli, M. Krisch, G. Ruocco, M. Santoro, and T. Scopigno, Nat. Phys. **6**, 503 (2010).
[56] F. Ritort and P. Sollich, Adv. Phys. **52**, 219 (2003).
[57] S. Whitelam, L. Berthier, and J. P. Garrahan, Phys. Rev. Lett. **92**, 185705 (2004).
[58] B. Martorell, L. Vocadlo, J. Brodholt, and I. G. Wood, Science **342**, 466 (2013).
[59] Y. Wang, J. Wang, A. Hermann, C. Liu, H. Gao, E. Tosatti, H.-T. Wang, D. Xing, and J. Sun, Phys. Rev. X **11**, 011006 (2021).